Applied Catalysis B: Environmental 325 (2023) 122395

Contents lists available at ScienceDirect

Applied Catalysis B: Environmental

journal homepage: www.elsevier.com/locate/apcatb

Effects of Al distribution in the Cu-exchanged AEI zeolites on the reaction performance of continuous direct conversion of methane to methanol

Peipei Xiao [a], Yong Wang [a], Yao Lu [a], Trees De Baerdemaeker [b], Andrei-Nicolae Parvulescu [b], Ulrich Müller [b], Dirk De Vos [c], Xiangju Meng [d], Feng-Shou Xiao [e], Weiping Zhang [f], Bernd Marler [g], Ute Kolb [h], Hermann Gies [a], Toshiyuki Yokoi [a,*]

[a] Institute of Innovative Research, Tokyo Institute of Technology, 4259 Nagatsuta, Midori-ku, Yokohama 226–8503, Japan
[b] Process Research and Chemical Engineering, BASF SE, Ludwigshafen 67056, Germany
[c] Center for Surface Chemistry and Catalysis, K. U. Leuven, Leuven 3001, Belgium
[d] Department of Chemistry, Zhejiang University, Hangzhou 310028, China
[e] College of Chemical and Biological Engineering, Zhejiang University, Hangzhou 310027, China
[f] State Key Laboratory of Fine Chemicals, School of Chemical Engineering, Dalian University of Technology, Dalian 116024, China
[g] Institute of Geology, Mineralogy und Geophysics, Ruhr-University Bochum, Bochum 44780, Germany
[h] Institute of Physical Chemistry, Johannes Gutenberg-University Mainz, Mainz 55128, Germany

ARTICLE INFO

Keywords:
AEI zeolite
Al distribution
Cu speciation
Acidic properties
Methane to methanol

ABSTRACT

The effects of the organic structure-directing agent (OSDA) with or without Na cations for the synthesis of AEI zeolite on the location and content of the Al atoms in the framework as well as the Cu speciation and acidic features of the exchanged Cu/AEI zeolite catalysts and their catalytic properties in the continuous direct conversion of methane to methanol (cDMTM) were investigated. The AEI zeolite synthesized with Na cations led to more Al and a higher percentage of Al pairs than the one prepared without Na cations. Consequently, the Cu/AEI zeolite catalysts synthesized with Na cations exhibited lower apparent activation energy of methane conversion, higher methanol formation rate, and less stable ability in the cDMTM reaction due to the more active dicopper species and higher acid amount than those prepared without Na cations. Adjustment of the close Al content in the framework of the two AEI zeolites by calcination, the Cu/AEI zeolite synthesized with Na cations evidenced a higher methanol selectivity and more stable reaction performance because of the different relationship between Cu species and acid sites, such as the distance, caused by the Al distribution. The methanol formation rate of 27.3 $\mu mol \cdot g^{-1} \cdot min^{-1}$ with about 50% selectivity and stable performance in the cDMTM reaction at 350 °C were obtained. Moreover, the stability of both 5Cu/AEI zeolite catalysts could be upgraded by further calcination to diminish the acid amount, the high methanol formation rate of the 5Cu/AEI zeolite synthesized with Na cations was maintained and the reaction stability was newly attained. The 5Cu/AEI zeolite synthesized without Na cations, merely the stable performance was reached, while the methanol formation rate and selectivity seriously declined. This work contributed to the development of AEI zeolite with different Al distributions and its significant impacts on the Cu speciation and acidic properties, thus providing a valuable strategy to obtain a robust Cu/AEI zeolite catalytic system for efficient and stable methanol production from methane.

1. Introduction

Zeolites are aluminosilicate molecular sieves that contain some fraction of framework Al^{3+} to substitute Si^{4+}, which makes the tetrahedron $[AlO_4]^-$ anionic lattice charge capable of balancing various extra framework cations, such as protons and transition metal cations that can serve as the catalytic active sites.[1] It is unanimously considered that the substitution of the framework Al among different crystallographically unique tetrahedral sites (T site) and in different degrees can bring out the extra framework cationic species of different strength and reactivity.[2] The unique T site and the degree of replacement determine the location and the content of Al atoms in the framework. Obviously, the two factors directly influence the extra framework cationic species. Thus, the control of Al atoms in the framework is particularly

* Corresponding author.
E-mail address: yokoi@cat.res.titech.ac.jp (T. Yokoi).

https://doi.org/10.1016/j.apcatb.2023.122395
Received 31 October 2022; Received in revised form 8 December 2022; Accepted 8 January 2023
Available online 11 January 2023

important for catalytic performance.[3,4] Particularly, the Al distribution of acid zeolite catalysts has been reported to influence the catalytic rates of n-alkane cracking,[5] the products selectivity,[6] and catalytic lifetime.[4] Furthermore, the distribution of Al atoms in the framework has been well recognized to influence the ability of exchange with various types of extra framework metal ions that act as precursor or active sites for partial oxidation of methane,[7,8] decomposition of nitrogen oxides,[9,10] dehydrogenation of light alkanes,[11] dehydroaromatization of methane,[12] and aromatization of methanol.[13] Additionally, the Al arrangement has also been associated with the adsorption performance of CO_2,[14] and hydrothermal stability.[15,16].

On account of the importance of Al distribution, great attempts have been made in the synthesis strategy to control the location of Al atoms in various zeolites.[17–20] The policy of using different OSDAs in the presence or absence of Na cations has been widely adopted in the synthesis of FER,[21,22] CHA,[23–25] and MFI zeolites[2,26,27]. Besides, the size and electrical properties of OSDAs and cations are also vital factors to arrange the Al distribution.[4,28] It is possible to change the location of Al atoms by adjusting the sources of Si, Al, and cations.[29–31] However, the abovementioned approaches are seldomly reported in the synthesis of AEI zeolite. The AEI-type aluminosilicate zeolite, i.e. SSZ-39, with three-dimensional 8-ring micropore (aperture size of 3.8 × 3.8 Å) and medium size cages that can include spheres up to 7.3 Å,[32] has exhibited splendid catalytic competence in the NH_3-SCR,[33] MTO,[16] and partial oxidation of methane,[34,35] which is regarded as an extremely promising small-pore zeolite.[36] Since it is extremely harsh on the synthetic conditions as well as the range of Si/Al ratio in the solid AEI zeolite is quite narrow (about 7–15).[32,37] The limited reports about the regulation of Al distribution for AEI zeolite are about OSDAs[32,38] and the starting materials[37,39].

The continuous direct conversion of methane to methanol (cDMTM) route is a new and significant branch of DMTM, [40-42] which is possible to circumvent the high energy consumption of indirect process and directly obtain methanol and other value-added chemicals from methane with lower energy consumption.[43–45] In comparison with the stepwise DMTM (sDMTM),[46,47] cDMTM possesses the characteristics of simple operation, real-time and comprehensive analysis for the products.[40–42] Because the products are in real-time and online analysis, rather than intermittently analyzing the accumulated results over a period of time, there are relatively high requirements on the amount of the products and the analytical instrument. [42] In order to reach the minimum limit of instrument detection, stronger oxidants such as N_2O and higher temperatures are usually required.[34,42] Continuous observation of the products led us to recognize that this is a tandem reaction under the premise of residual acid amount, first methane conversion to methanol and then methanol production to olefins. In order to obtain high methanol yield, the acid amount needs to be controlled and the activity of metal species should be maximized as much as possible. In the current restricted reports, copper zeolite catalysts are frequently utilized.[34,35,40,41,42] However, because of the difficulty of regulating the distribution and content of Al atoms in the AEI zeolite, publications about the effects of Cu speciation and acidic features caused by the Al distribution in the AEI zeolite on the cDMTM reaction performance were rare.

In this work, the AEI-type aluminosilicate zeolites were synthesized under the guidance of OSDA with or without Na cations in the premise of the same total amount of cations. To our best knowledge, this is the first report about regulating the Al distribution of AEI zeolite using Na cations. The ^{27}Al MAS NMR, ^{29}Si MAS NMR, and the Co^{2+}-exchange methods were adopted to explore the location of Al atoms in the framework. The exchanged Cu/AEI zeolites displayed different Cu speciation and acidic features. Thereafter, the Cu/AEI zeolite catalysts were applied in the cDMTM reaction at 300–450 °C to calculate the activation energy and optimize the reaction temperature. The stability of the Cu/AEI zeolites was compared at the optimum temperature (350 °C). Worth noting was that the different contents and locations of Al atoms between the two AEI zeolites were attributed to the Na cations. The attempts to regulate the matching Al content in the framework of the AEI zeolites were made by calcination to investigate the influence of the Al environment on the reaction performance. Moreover, the exchange between as-synthesized AEI zeolites and $Cu(NO_3)_2$ solution was carried out to reflect the original Al distribution. Finally, the stability in the cDMTM reaction of the Cu/AEI zeolites was improved by further calcination to reduce the acid amount.

2. Experiments

2.1. Catalysts preparation

The AEI-type aluminosilicate zeolites were prepared by using *N,N*-dimethyl-3,5-dimethylpiperidinium hydroxide (DMDMP) as OSDA. The AEI zeolites synthesized in the presence or absence of Na cations were remarked as AEI(Na) and AEI(Na free), respectively. In a typical synthesis of AEI(Na), DMDMP was mixed with the sodium hydroxide aqueous solution. Then, zeolite Y (CBV-780, Si/Al=40) acted as both alumina and silica sources was added to the above solution. The prepared gel with the molar ratio of 1 SiO_2: 0.0125 Al_2O_3: 0.155 OSDA: 0.48 NaOH: 31 H_2O was crystallized at 150 °C in a rotating oven for 3 days. The synthesis of AEI(Na free) was similar to that of AEI(Na), just using the gel with molar ratio of 1 SiO_2: 0.0125 Al_2O_3: 0.635 OSDA: 10 H_2O to crystallize at 150 °C in a rotating condition for 7 days. The obtained as-synthesized products were filtered, dried at 100 °C, and calcined at 550 °C in air for 10 h to remove the OSDA. The ion-exchange was carried out twice to obtain NH_4-form zeolite using 2.5 M NH_4NO_3 aqueous solution in a stirring condition at 80 °C for 3 h.

The exchanged Cu/AEI zeolite catalysts with various copper loadings were prepared by changing the concentration of $Cu(NO_3)_2$ solution. Typically, 1 g NH_4-form AEI was ion-exchanged with 100 ml of 1, 5, 50 mmol/L $Cu(NO_3)_2$ aqueous solution at 80 °C for 24 h. The solid product was washed, dried, and calcined at 550 °C for 5 h in air. The obtained samples were denoted as *x*Cu/AEI(Na) and *x*Cu/AEI(Na free), where *x* corresponds to the concentration of $Cu(NO_3)_2$ solution.

To regulate the Al content of the AEI(Na) zeolite in the framework close to that of AEI(Na free), the as-AEI(Na) was calcined at 850 °C for 10 h in air, followed by NH_4-exchange with 2.5 mol/L NH_4NO_3 solution and Cu-exchange with 5 mmol/L $Cu(NO_3)_2$ solution, the other process was similar with the above description. The obtained sample was remarked as 5Cu/AEI(Na)− 850.

Co^{2+}-exchanged AEI samples (Co/AEI(Na), Co/AEI(Na free), Co/AEI (Na)− 850) were prepared according to the literature.[4,48] First, the calcined AEI zeolites were ion-exchanged to Na/AEI with 1 mol/L $NaNO_3$ aqueous solution at 80 °C for 7 h. Then, the obtained Na/AEI samples were ion-exchanged with 0.05 mol/L $Co(NO_3)_2$ aqueous solution at 80 °C for 7 h. After Co^{2+}-exchange, the samples were filtered, washed with deionized water, and dried at 100 °C overnight. In order to eliminate operating errors, two parallel experiments were arranged. To prevent incomplete exchange, the 0.5 mol/L $Co(NO_3)_2$ aqueous solution was adopted to make another attempt. The proportion of Al pairs was the average of the above three results.

The details about the characterization and catalytic activity test are provided in the supporting information.

3. Results and discussion

3.1. Catalyst characterization

3.1.1. Structure and morphology

Fig. S1 shows the XRD pattern of the as-AEI zeolite samples. Both samples presented a series of characteristic peaks (9.4, 16.2, 16.9, 24.0°) associated with the AEI structure. The morphology of AEI(Na) and AEI (Na free) was inspected by the SEM, revealing the cuboid crystals with

Table 1
Summary of Al arrangement and distribution of the AEI zeolites.

Sample	Si/Al[a]	Co/Al[a]	Al_F (%)[b]	Al arrangement (%)		Al_F distribution (%)[c]			
				Al_p[d]	Al_i[e]	Q^4 (2Al)	Q^3 (0Al)	Q^4 (1Al)	Q^4 (0Al)
AEI(Na)	7.7	0.21	90	48	52	7	4	24	65
AEI(Na free)	10.1	0.13	88	31	69	4	6	19	71
AEI(Na)− 850	7.7	0.16	70	46	54	4	4	19	73

[a] by ICP-AES
[b] by deconvolution of the ^{27}Al MAS NMR spectrum
[c] by deconvolution of the ^{29}Si MAS NMR spectrum, Q^4(nAl) and Q^3(0Al) represent $Si(OSi)_{4-n}(OAl)_n$ and $Si(OH)\text{-}(OSi)_3$, respectively.
[d] by $Al_p = Al_p/Al_F = 2Comax/Al_F$
[e] by $Al_i = (Al_F\text{-}Al_p)/Al_F$

Table 2
Chemical composition and acidity of the Cu-exchanged AEI zeolites.

Sample	Chemical Compositions[a]			Acidity by NH_3-TPD (mmol/g)[b]			
	Si/Al	Cu/Al	Cu (wt%)	Weak	Medium	Strong	Total
1Cu/AEI(Na)	7.3	0.03	0.31	0.45	0.44	0.46	1.35
5Cu/AEI(Na)	7.4	0.07	0.78	0.37	0.59	0.42	1.39
50Cu/AEI(Na)	7.5	0.19	2.13	0.28	1.04	0.28	1.59
1Cu/AEI(Na free)	10.0	0.06	0.55	0.31	0.39	0.34	1.04
5Cu/AEI(Na free)	9.7	0.10	0.89	0.31	0.58	0.33	1.22
50Cu/AEI(Na free)	9.7	0.22	2.04	0.19	0.77	0.33	1.28
5Cu/AEI (Na)− 850	7.2	0.06	0.75	0.18	0.53	0.43	1.14
cal-5Cu/as-AEI(Na)	7.3	0.12	1.35	0.47	0.29	0.34	1.10
cal-5Cu/as-AEI(Na free)	9.9	0.05	0.43	0.38	0.34	0.35	1.07
[5Cu/AEI (Na)]− 750	7.4	0.07	0.78	0.20	0.45	0.46	1.11
[5Cu/AEI(Na free)]− 750	9.7	0.10	0.89	0.14	0.46	0.33	0.93

[a] by ICP-AES.
[b] by NH_3-TPD; fitting curves of the weak, medium, strong acid sites were calculated at approximately 160, 300 and 475 °C, respectively.

the size of about 200 nm * 500 nm* 500 nm and 300 nm * 600 nm* 600 nm, respectively (Fig. S2). Furthermore, the textural properties of the samples were investigated by N_2 adsorption and desorption (Fig. S3), verifying that both samples have a close BET surface area and micropore volume (Table S1). It is worth mentioning that similar morphology and textural properties are convenient to compare the influence of different locations and contents of Al atoms on the acidic properties and Cu speciation. Fig. S4 discloses the thermal analysis (TG-DTA) of the as-synthesized zeolite samples. Both AEI(Na) and AEI(Na free) zeolite samples exhibited major exothermic peaks at 250–800 °C, accompanied by a weight loss of about 15.3% and 17.2%, respectively, as a result of the decomposition of OSDA. The chemical composition of all the samples analyzed by ICP-AES is listed in Table 2 and S4. The Si/Al molar ratio of AEI(Na) and AEI(Na free) was 7.7 and 10.1, respectively. The higher Al content of AEI(Na) verified the flexibility of Na cations in balancing the tetrahedron $[AlO_4]^-$ anionic lattice charge.

3.1.2. Al distribution

The Al distribution in the AEI zeolites was first identified by ^{27}Al MAS NMR. From the ^{27}Al MAS NMR spectra (Fig. S5), both AEI(Na) and AEI(Na free) exhibited a sharp band at 58 ppm corresponding to the four-coordinated aluminum (Al_{IV}) in the zeolite framework and a weak band at 0 ppm associating to six-coordinated extra framework Al (Al_{VI}). [49] By deconvolution of the ^{27}Al MAS NMR spectra (Fig. S5), the proportion of Al in the framework (Al_{IV} or Al_F) for AEI(Na) and AEI(Na free) was calculated from the peak area of Al_{IV} at 70–40 ppm as 90% and 88%, respectively. It has been well recognized that the Al_F can be categorized as isolated Al atom (Al_i) and Al pairs (Al_p). The Al_p represents two Al atoms located in one ring at an interval of less than three (-Si-O-) groups, which can be balanced by Co^{2+} cations.[50] While the Al_i shares more than three (-Si-O-) groups, which is poor accommodation of Co^{2+} species.[50] The proportion of Al_p for AEI(Na) and AEI(Na free) was calculated as 48% and 31% (Table 1 and S2), respectively, using the method of Dedecek et al. and referring to our previous work. [2,4] Since the location of Al atoms was dependent on the size and type of cations,[23,27] the difference in Al distribution between the AEI(Na) and AEI(Na free) zeolites caused by the presence or absence of Na cations. The result was verified by the higher percentage of Q4(1Al) and Q4 (2Al) for AEI(Na), which was calculated from the area of the corresponding peaks in the ^{29}Si MAS NMR spectra (Fig. S6 and Table 1).[49].

Considering the contents of Al, Na, and OSDA in the AEI zeolites can be measured by ICP-AES, AAS, and TG-DTA, respectively. Simultaneously, it was known that per unit cell contains 4 cages for the AEI zeolite.[51] The contents of Al, Na, and OSDA in per cage of the AEI zeolites can be calculated (Table S3). The total cations per cage, i.e. the (ODSA+Na) content for the AEI(Na) and AEI(Na free) zeolites was 1.72 and 0.96/cage, respectively. It is to be noted that the total (ODSA+Na) in the synthesis gel of the two zeolites was the same. However, the Al content of AEI(Na) was higher than that of AEI(Na free) since there were more cations species on the extra framework to balance the tetrahedron $[AlO_4]^-$ anionic lattice charge. The result confirmed that the smaller size of Na cations has the advantage of balancing Al in spatial position, thus bringing about more Al and a higher percentage of Al_p, which was in keeping with the situation of MFI and CHA zeolites synthesized in the presence of OSDA with or without Na cations.[23,27].

3.1.3. Acidic properties

The acidic properties of the samples were analyzed by NH_3-TPD (Fig. S7). The NH_3-TPD spectra were deconvoluted into three peaks centered around 150, 300, and 475 °C, which corresponds to the physically adsorbed NH_3, the medium acid sites derived from the NH_3 adsorbed on the Lewis acid sites (LAS), and the strong acid sites related with the NH_3 adsorbed on the Brønsted acid sites (BAS) (Si−OH−Al), respectively.[52,53] The acid amount estimated from the fitting peak area of NH_3-TPD profiles is listed in Table 2 and S4. Obviously, for the two kinds of AEI zeolites, with the Cu content increasing, the strong acid amount dropped owing to the replacement of proton from (Si−OH−Al) by Cu^{2+}, and the medium acid amount heightened because of the cumulative Cu content. The results were in line with the literature. [54] Meanwhile, the total acid amount of the *x*Cu/AEI(Na) zeolite catalysts was higher than that of the *x*Cu/AEI(Na free) samples under the close Cu content due to the higher Al content of AEI(Na) zeolite.

In addition, the FTIR spectra in the region of hydroxyl stretching vibration were employed to reflect the acidic features of the Cu/AEI zeolites (Fig. S8). The bands at 3745, 3657, and 3616 cm^{-1} with a shoulder at 3585 cm^{-1} were assigned to the silanol groups, Al-OH and Cu-OH on the extra framework, and the Si–OH–Al bridging hydroxyl groups, respectively.[55,56] The obvious difference between *x*Cu/AEI

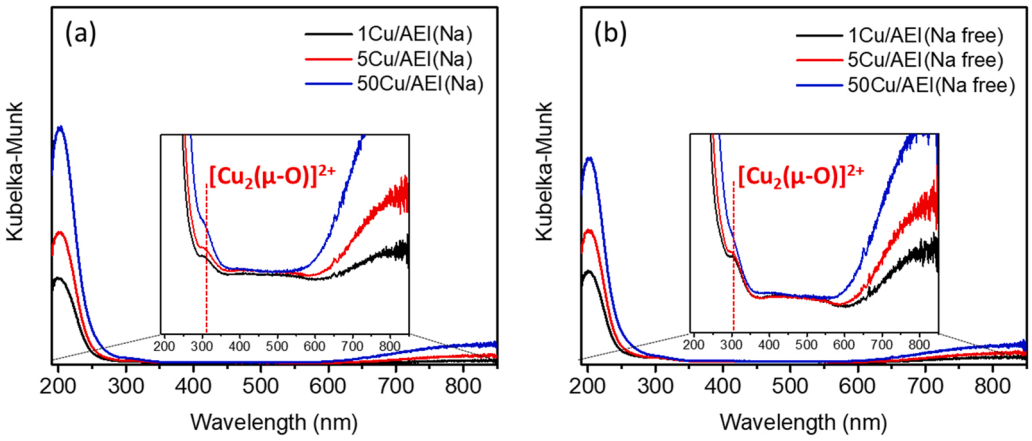

Fig. 1. UV–vis spectra of (a) *x*Cu/AEI(Na) and (b) *x*Cu/AEI(Na free) zeolite catalysts.

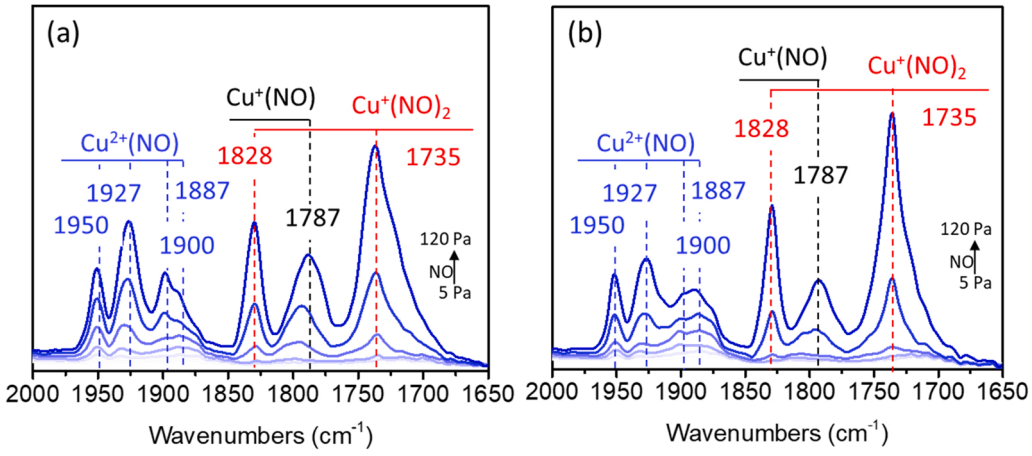

Fig. 2. NO (5–120 Pa) adsorption FTIR spectra over (a) 5Cu/AEI(Na) and (b) 5Cu/AEI(Na free) zeolite catalysts collected at − 120 °C after activation at 500 °C in vacuum for 1 h.

(Na) and *x*Cu/AEI(Na free) was the intensity of the band belonging to the bridging hydroxyl groups. Moreover, the intensity of the band at 3616 cm^{-1} for both *x*Cu/AEI(Na) and *x*Cu/AEI(Na free) zeolites was condensed with *x* increasing because of the replacement of hydrogen in Si–OH–Al by Cu ions, which has been confirmed by the NH_3-TPD results.

3.1.4. Cu speciation

The Cu speciation of the Cu/AEI samples was first evaluated by UV–vis spectroscopy. Fig. 1 presents that both *x*Cu/AEI(Na) and *x*Cu/AEI(Na free) zeolite catalysts exposed an intense absorption band at 210 nm, which was attributed to the O → Cu^{2+} charge transfer (CT)

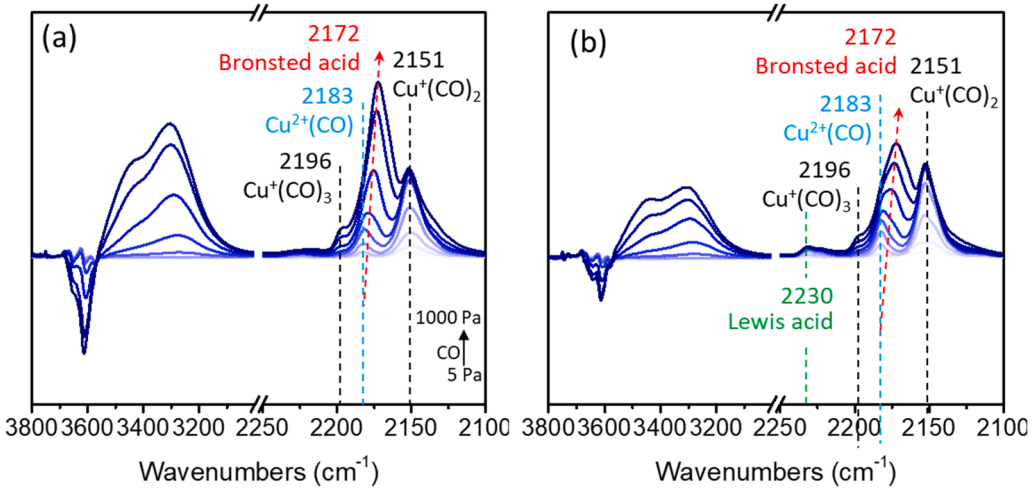

Fig. 3. CO (5–1000 Pa) adsorption FTIR spectra over (a) 5Cu/AEI(Na) and (b) 5Cu/AEI(Na free) zeolite catalysts collected at − 120 °C after activation at 500 °C in vacuum for 1 h.

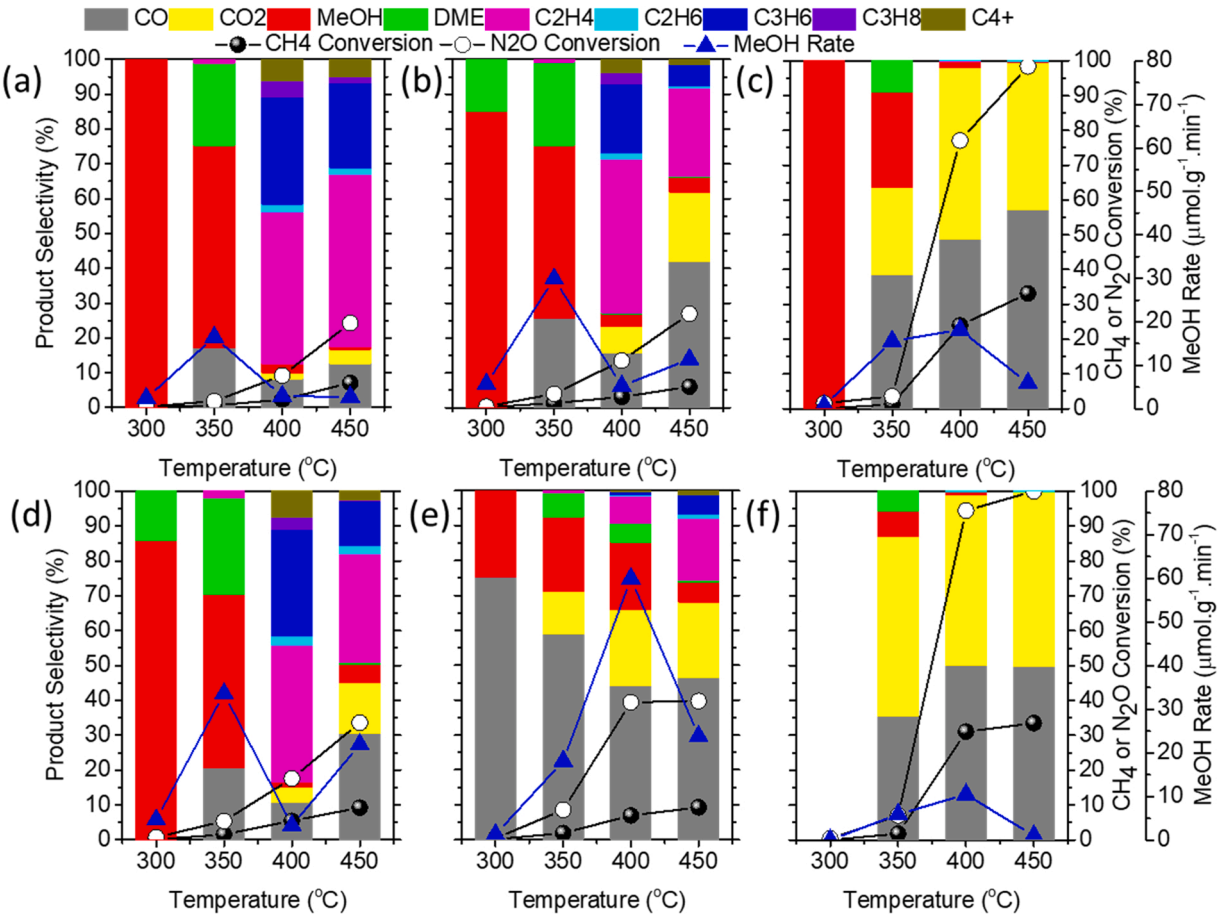

Fig. 4. Effects of reaction temperature on the cDMTM reaction performance over (a) 1Cu/AEI(Na), (b) 5Cu/AEI(Na), (c) 50Cu/AEI(Na), (d) 1Cu/AEI(Na free), (e) 5Cu/AEI(Na free) and (f) 50Cu/AEI(Na free) zeolite catalysts. Reaction conditions: 300–450 °C, 100 mg catalyst, $CH_4/N_2O/H_2O/Ar$ = 10/10/2/3 ml min^{-1}, SV = 15000 ml·g^{-1} h^{-1}.

transitions in the isolated Cu species.[57,58] The weak absorption band at 320 nm was related to the dimeric Cu species, i.e. mono-(μ-oxo) dicopper(II) ($[Cu_2(\mu\text{-}O)]^{2+}$) complexes.[59].

Furthermore, NO adsorption FTIR spectroscopy at − 120 °C was introduced to access the variations in the copper oxidation state and most importantly to qualitatively and quantitatively identify the binuclear copper species.[60] As demonstrated in Fig. 2 and S9, the bands at 1828, 1735, and 1787 cm^{-1} are associated with NO bound to Cu^+ sites, as well as at 1887, 1900, 1927, and 1950 cm^{-1} are assigned to different Cu^{2+} species.[61] According to Bokhoven et al., [61] the bands at 1887 and 1900 cm^{-1} are related to the adsorption of a single NO molecule on the $[Cu(OH)]^+$ species, while the bands at 1927 and 1950 cm^{-1} are corresponding to the adsorption of a single NO molecule on the dimeric copper species.[61] The peak intensity is related to the amount of the corresponding copper species. Apparently, the intensity of the band at 1927 cm^{-1} for 5Cu/AEI(Na) was stronger than that of 5Cu/AEI(Na free) and the intensity of the band at 1950 cm^{-1} for 5Cu/AEI(Na) was similar to that of 5Cu/AEI(Na free), signifying the fact that the amount of dimeric copper species in 5Cu/AEI(Na) was higher than that of 5Cu/AEI (Na free) (Fig. 2). Besides, the NO adsorption FTIR spectra for 50Cu/AEI samples presented the similar rule (Figs. S9(c and d)). We attributed the stronger intensity of bands at 1950 and 1927 cm^{-1} for 1Cu/AEI(Na free) than that of 1Cu/AEI(Na) to the much higher Cu content (Figs. S9(a and b)).

In addition, CO adsorption FTIR spectroscopy at − 120 °C was adopted to simultaneously clarify the acidic and Cu sites.[62] As revealed in Fig. 3 and S10, at low CO coverages, the exclusive formation of $Cu^+(CO)_2$ at 2151 cm^{-1} and $Cu^{2+}CO$ at 2183 cm^{-1} were observed. [63] Increasing the CO pressure led to the appearance of a new band assigned to $Cu^+(CO)_3$ at 2196 cm^{-1}.[62] As the CO pressure continued to increase, the band at 2183 cm^{-1} blue-shifted to 2172 cm^{-1}, which was assigned to the υ_{C-O} vibration of adsorbed CO interacting with zeolitic OH groups via the weak hydrogen bonds.[64] Concomitant with the development of these bands was the appearance of a broad feature centered at 3300 and 3430 cm^{-1}, and the negative features in the vibrational region of zeolitic OH groups centered at 3600 and 3640 cm^{-1}. The intensity of the peaks at 2183 and 2196 cm^{-1} for 5Cu/AEI(Na) and 5Cu/AEI(Na free) are different from each other, signifying the different Cu speciation and locations (Fig. 3). Additionally, 5Cu/AEI(Na free) presented a weak band at 2230 cm^{-1}, which was assigned to the LAS. It was speculated that the band came from the Al species on the extra framework (Al_{EF}) since the same band was also observed on H-AEI(Na free) and the other *x*Cu/AEI(Na free) zeolite catalysts (Figs. S10(b, d, f)). Moreover, the BAS amount of *x*Cu/AEI(Na) at 2172 cm^{-1} was obviously higher than that of *x*Cu/AEI(Na free) under the corresponding Cu content due to the more Al content in the framework, which was consistent with the NH_3-TPD results.

3.2. Catalytic performance

3.2.1. Effects of reaction temperature

The reaction performance of cDMTM was first evaluated at 300–450 °C (Figs. S11 and S12). The formation route of all the products and the possible reaction mechanism have been clarified (Fig. S13). Fig. 4 shows the reaction performance, both the methane and N_2O conversion were developed along with the reaction temperature and the

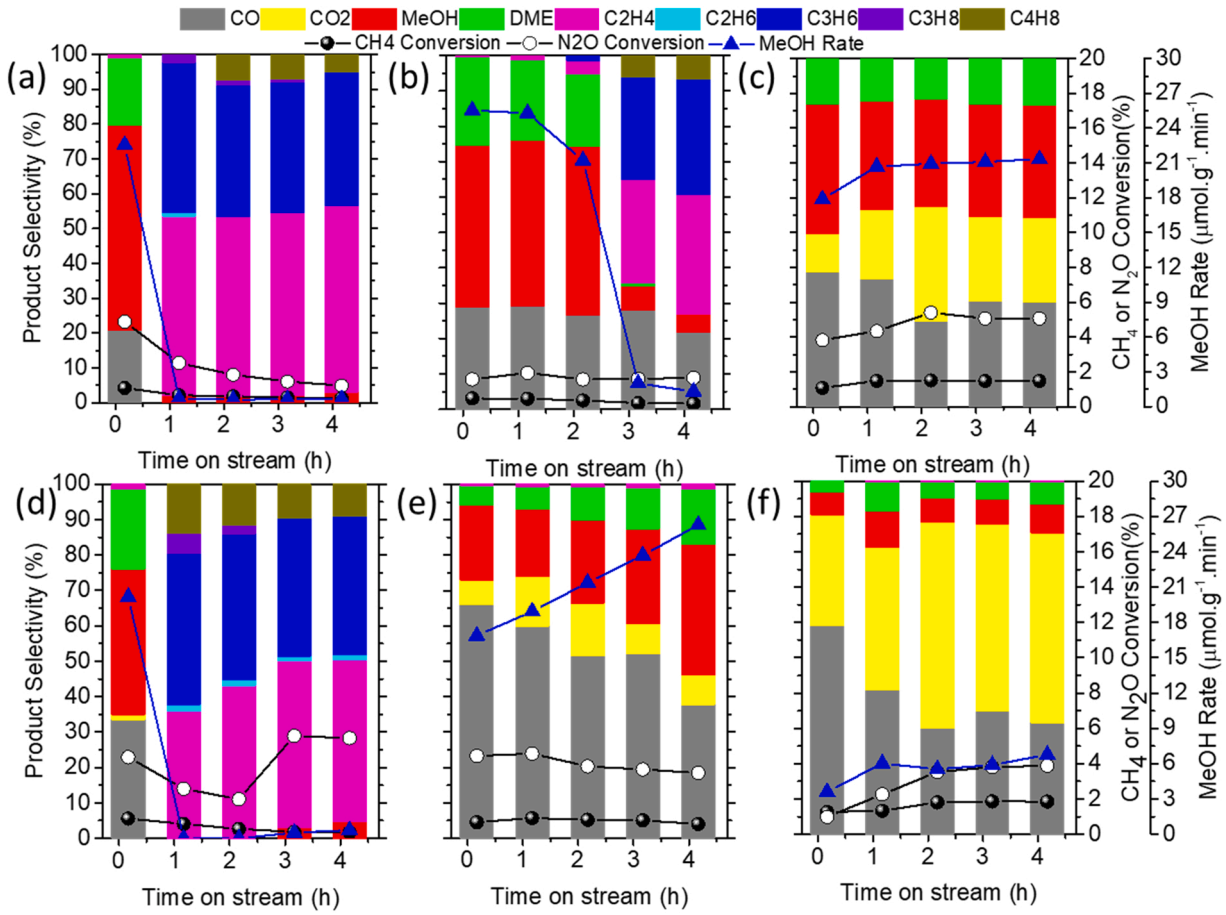

Fig. 5. The stability of (a) 1Cu/AEI(Na), (b) 5Cu/AEI(Na), (c) 50Cu/AEI(Na), (d) 1Cu/AEI(Na free), (e) 5Cu/AEI(Na free) and (f) 50Cu/AEI(Na free) zeolite catalysts in cDMTM reaction at 350 °C. Reaction conditions: 100 mg catalyst, $CH_4/N_2O/H_2O/Ar = 10/10/2/3$ ml min^{-1}, SV = 15000 ml·g^{-1} h^{-1}.

Cu content. For the two 1Cu/AEI zeolites, the main products were methanol and dimethyl ether (DME) at 300 and 350 °C, and the olefins turned to the main products as the temperature raised to 400 and 450 °C. The huge gaps appeared between the two 5Cu/AEI zeolites. As we can see, the product distribution of 5Cu/AEI(Na) was still similar to that of 1Cu/AEI(Na) except for the enlarged selectivity of CO_2 and CO at 400 and 450 °C. However, the selectivity of CO for 5Cu/AEI(Na free) was greatly advanced at 300–450 °C in comparison with 5Cu/AEI(Na) and 1Cu/AEI(Na free). With regard to 50Cu/AEI(Na), the selectivity of MeOH at 300 and 350 °C was 100% and 27.3%, respectively, however, when the temperature grew to 400 and 450 °C, the total selectivity of CO and CO_2 was up to 98.1% and 99.5%, respectively. Note that no product for 50Cu/AEI(Na free) was observed at 300 °C, meanwhile, the total selectivity of CO and CO_2 was higher than 85% at 350–450 °C. The reaction results were related to the content and distribution of Al atoms, i.e. the acidic features and Cu speciation. Under the low Cu content (1Cu/AEI), it was the acid sites that played the main role. Hence, the product distribution of the two 1Cu/AEI zeolites was analogous. When the concentration of $Cu(NO_3)_2$ solution was enhanced to 5 mmol/L, the strong acid amount of 5Cu/AEI(Na) was still high to 0.42 mmol/g. That is, the acid amount and the Cu species were evenly matched. Consequently, the product distribution of 5Cu/AEI(Na) was similar to that of 1Cu/AEI(Na), but the conversion of CH_4 and N_2O, as well as the formation rate of MeOH for 5Cu/AEI(Na), were higher than that of 1Cu/AEI(Na). On the contrary, oxidation caused by the Cu species was greater than the acid site for the 5Cu/AEI(Na free) zeolite due to the less Al content of the parent H-AEI(Na free) zeolite. As a result, CO became the main product instead of olefins and MeOH. Further rising the Cu concentration to 50 mmol/L, the Cu species played a major role in place of the acid sites for the 50Cu/AEI zeolites. As a consequence of the oxidation property of Cu species, the produced MeOH was easy to oxidation and overoxidation to CO and CO_2, respectively. For comparison, the activation energy (*Ea*) of methane conversion was calculated based on the Arrhenius equation.[41] Figs. S14 and S15 illustrate that the 5Cu/AEI(Na) and 5Cu/AEI(Na free) zeolites achieved the lowest *Ea* among the *x*Cu/AEI(Na) and *x*Cu/AEI(Na free) zeolites, implying that the balance between acidic features and Cu speciation was important for acquiring lower activation energy. The *Ea* of *x*Cu/AEI(Na) was found less than that of *x*Cu/AEI(Na free) except for the 1Cu/AEI zeolites. Noteworthy, the gap between CH_4 conversion and N_2O conversion was due to the different calculation methods (see supporting information).

3.2.2. *Catalytic stability*

Due to the considerable methanol formation rate, methanol selectivity, and methane conversion at various Cu contents, the catalytic stability in the cDMTM reaction was assessed at 350 °C (Figs. S11 and S16). As shown in Fig. 5(a and d), the initial MeOH formation rate of the 1Cu/AEI zeolites was higher than 20 mmol·g^{-1}·min^{-1}. However, the produced MeOH was quickly and massively converted into olefins at the second point (the 1.17th h). Because of the difference in acid amount and acid species between 1Cu/AEI(Na) and 1Cu/AEI(Na free) zeolites, the distribution of olefins was different. Notably, the reason for the different reaction performance at 350 °C between Fig. 5 and Fig. 4 was that the fresh catalysts were utilized in Fig. 5, while the used catalysts were reprocessed after activation at 500 °C for 1 h in Fig. 4. When the concentration of the $Cu(NO_3)_2$ solution was increased to 5 mmol/L (Fig. 5(b and e)), the initial formation rate and selectivity of MeOH for 5Cu/AEI(Na) was 25.3 mmol·g^{-1}·min^{-1} and 46%, respectively.

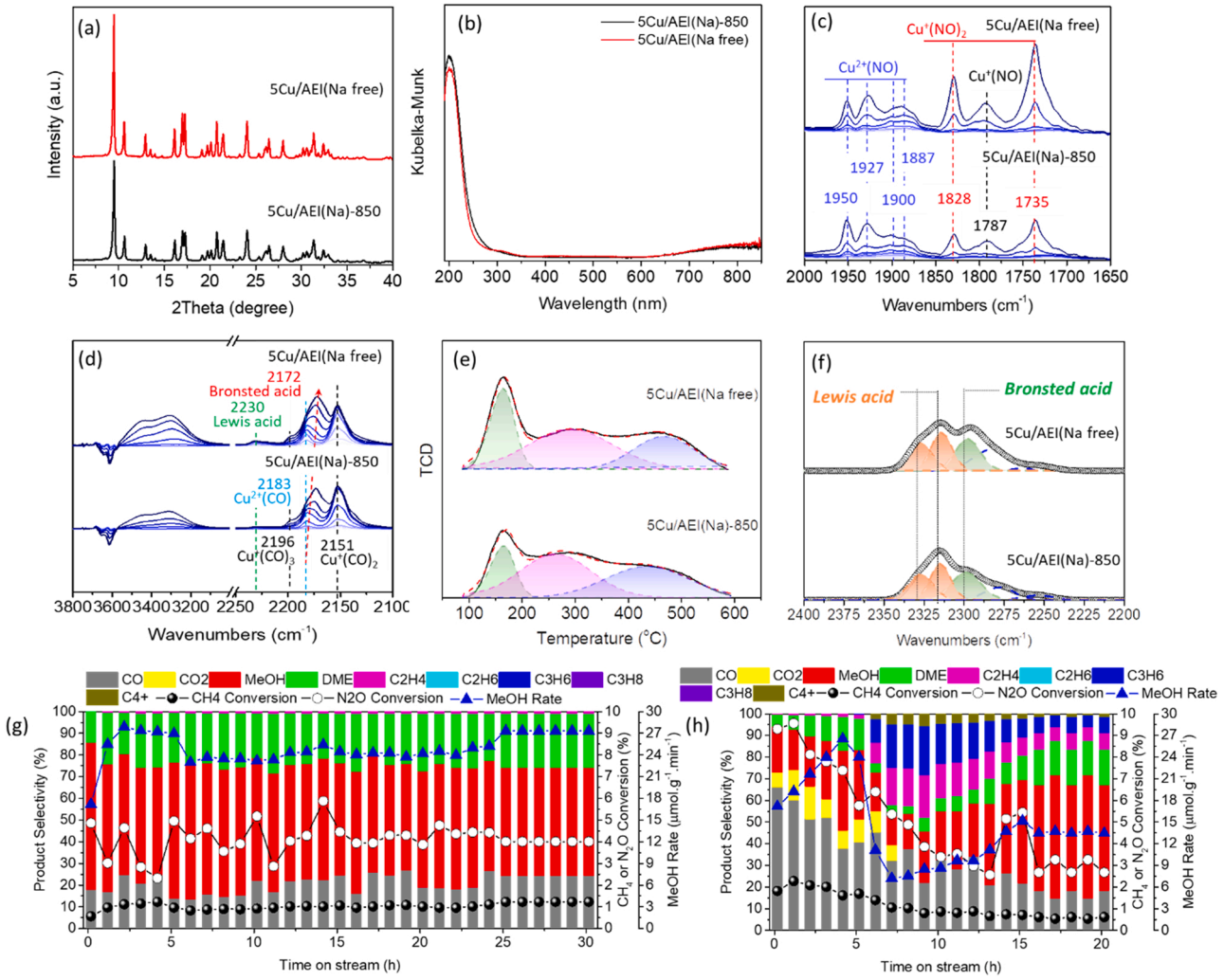

Fig. 6. (a) XRD patterns and (b) UV–vis spectra for 5Cu/AEI(Na)− 850 and 5Cu/AEI(Na free) zeolite catalysts. (c) NO (5–120 Pa) adsorption FTIR spectra and (d) CO (5–1000 Pa) adsorption FTIR spectra over 5Cu/AEI(Na)− 850 and 5Cu/AEI(Na free) zeolite catalysts zeolite catalysts collected at − 120 °C after activation at 500 °C in vacuum for 1 h. (e) NH_3-TPD spectra for 5Cu/AEI(Na)− 850 and 5Cu/AEI(Na free) zeolite catalysts. (f) CD_3CN (200 Pa) adsorption FTIR spectra over 5Cu/AEI (Na)− 850 and 5Cu/AEI(Na free) zeolite catalysts at room temperature after activation at 350 °C in vacuum for 3 h. The performance of (g) 5Cu/AEI(Na)− 850 and (h) 5Cu/AEI(Na free) zeolite catalysts in the cDMTM reaction at 350 °C. Reaction conditions: 100 mg catalyst, $CH_4/N_2O/H_2O/Ar$ = 10/10/2/3 ml·min^{-1}, WHSV = 15000 ml·g^{-1}·h^{-1}.

However, MeOH began to massively convert to olefins after 3 h. Nonetheless, a small amount of MeOH was retained (MeOH selectivity of 5.3%), probably ascribable to the insufficient amount of acid sites leading to incomplete conversion of methanol. On the contrary, the formation rate and selectivity of MeOH for 5Cu/AEI(Na free) were constantly elevated within the 5 h from 17.2 mmol·g^{-1}·min^{-1} and 21% to 26.5 mmol·g^{-1}·min^{-1} and 37%, respectively. The significantly different reaction results also lie in the variance of acidic features and copper species between the two 5Cu/AEI zeolites. 5Cu/AEI(Na) possessed more dicopper species than 5Cu/AEI(Na free), which meant higher activity in activation of methane to methanol. Simultaneously, 5Cu/AEI(Na) contained more acid amount (Table 2 and S5) than 5Cu/AEI(Na free), indicating that the reaction of methanol to olefins eventually occurred on the two 5Cu/AEI samples as the reaction proceeds, and it was earlier on 5Cu/AEI(Na) than 5Cu/AEI(Na free). Finally, both 50Cu/AEI zeolites achieved stable product distribution and reactant conversion, however, the formation rate and selectivity of MeOH for 50Cu/AEI(Na) (21.3 mmol·g^{-1}·min^{-1} and 32%) were much higher than that of 50Cu/AEI(Na free) (6.8 mmol·g^{-1}·min^{-1} and 8%) (Fig. 5(c and f)). The higher CO_2 selectivity obtained by 50Cu/AEI(Na free) was possibly due to the shorter distance between two active Cu species. In other words, the produced methanol on one Cu site was transported to the proximate Cu site and over-oxidized to CO_2.

3.2.3. Discussion

3.2.3.1. Regulation the similar Al content in the framework. The influence of Al distribution on the loaded Cu speciation has been discussed. [50] It is convenient to compare the effects caused by the different Al distributions when the Al content was consistent. However, in this study, both content and distribution of Al atoms were different. After several attempts, the Al content in the framework of AEI(Na) could be reduced by increasing the first-time calcination temperature to 850 °C, and the sample was named AEI(Na)− 850. The AEI topology structure of AEI (Na)− 850 was well preserved (Fig. 6a). Hereafter, the Al distribution of the H-type AEI(Na)− 850 was analyzed by NMR and Co^{2+}-exchange. As evidenced in Fig. S17, the proportion of Al_{IV} in the framework for H-AEI (Na)− 850 calculated from the peak area at 70–40 ppm of ^{27}Al MAS NMR spectrum was 70%. Combined with the result of Co^{2+}-exchange, the proportion of Al_p for H-AEI(Na)− 850 was calculated as 46% (Table 1 and S2). The high percentage of Al*p* depended on the high Co/Al ratio and the low share of Al_{IV}. It is worth pointing out that the

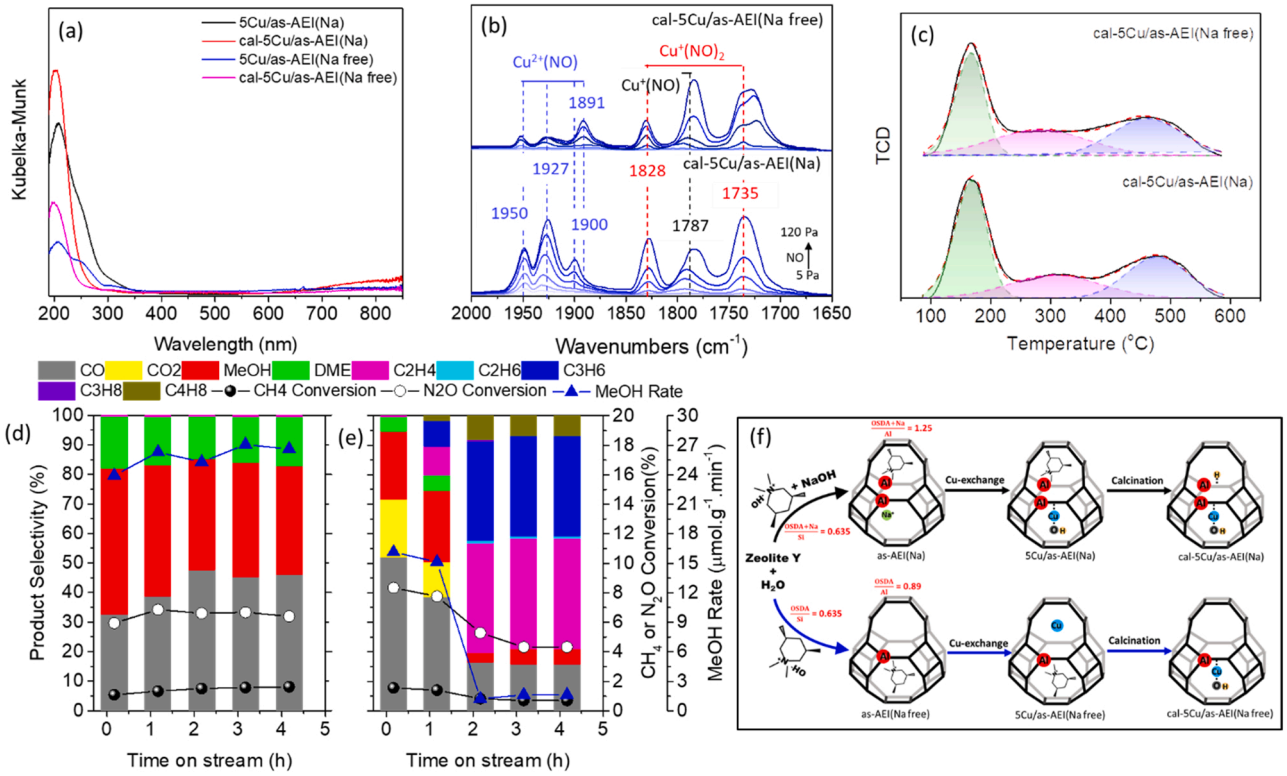

Fig. 7. (a) UV–vis spectra and (b) NO (5–120 Pa) adsorption FTIR spectra over cal-5Cu/as-AEI(Na) and cal-5Cu/as-AEI(Na free) zeolite catalysts collected at − 120 °C after activation at 500 °C in vacuum for 1 h. (c) NH_3-TPD spectra for cal-5Cu/as-AEI(Na) and cal-5Cu/as-AEI(Na free) zeolite catalysts. The performance of (d) cal-5Cu/as-AEI(Na) and (e) cal-5Cu/as-AEI(Na free) zeolite catalysts in the cDMTM reaction at 350 °C. Reaction conditions: 100 mg catalyst, $CH_4/N_2O/H_2O/Ar$= 10/10/2/3 ml·min^{-1}, WHS = 15000 ml·g^{-1}·h^{-1}. (f) The possible loading route of Cu ions on the as-synthesized AEI zeolites.

effects of the extra framework (Al_{VI}) and associate framework (Al_{V}) Al on the reaction performance were ignored in this study. The deconvolution of ^{29}Si MAS NMR result manifested that the percentage of Q4(1Al) and Q4(2Al) for H-AEI(Na)− 850 were the same with that of H-AEI(Na free) (Fig. S18 and Table 1). Afterward, the physicochemical properties, acidic features, Cu speciation, and stability in the cDMTM reaction at 350 °C of 5Cu/AEI(Na)− 850 and 5Cu/AEI(Na free) were carefully compared (Fig. 6 and S3, Table 2 and S1). The Cu content of 5Cu/AEI(Na)− 850 (0.75 wt%) was slightly lower than that of 5Cu/AEI(Na free) (0.89 wt%). The acid amount measured by NH_3-TPD displayed a little difference between 5Cu/AEI(Na)− 850 and 5Cu/AEI(Na free) (Fig. 6e and Table 2), especially in the amount of strong and weak acid sites. However, the amount of BAS and LAS detected by CD_3CN adsorption FTIR revealed a close value between 5Cu/AEI(Na)− 850 and 5Cu/AEI(Na free) (Fig. 6 f and Table S5). Additionally, the similar Cu species in both catalysts was confirmed based on UV–vis spectra (Fig. 6b), NO adsorption FTIR spectra (Fig. 6c), and CO adsorption FTIR spectra (Fig. 6d). As for the reaction performance at 350 °C, the MeOH formation rate of both catalysts increased from approximately 17 to 27 μmol·g^{-1}·min^{-1}. However, the interesting difference was the stability and selectivity of products. 5Cu/AEI(Na)− 850 showed a stable reaction performance within 30 h and about 55% of MeOH selectivity (Fig. 6g). On the contrary, the MeOH formation rate of 5Cu/AEI(Na free) drop from the peak value of 26.5 μmol·g^{-1}·min^{-1} to 7.2 μmol·g^{-1}·min^{-1} and final stabilized at 13.4 μmol·g^{-1}·min^{-1} (Fig. 6h). As well, the MeOH selectivity varied from the initial 21% to the final 49%. We speculated that the similar maximum MeOH formation rate ascribed to the alike dimeric copper species, but different stability and products selectivity between 5Cu/AEI(Na)− 850 and 5Cu/AEI(Na free) catalysts was due to the relationship between Cu species and acid sites, such as the distance, [65] caused by the different environment of Al atoms. Specifically, the distance between Cu species and acid sites in 5Cu/AEI(Na free) would be possibly shorter than that in 5Cu/AEI(Na)− 850 and longer than that in 5Cu/AEI(Na). Hence, it has been considered that the production time of olefins from methanol on 5Cu/AEI(Na free) was earlier than on 5Cu/AEI(Na)− 850 but later than on 5Cu/AEI(Na).

3.2.3.2. Cu-exchange with the as-AEI and cal-AEI zeolites. We assumed that the exchange between as-AEI zeolites and $Cu(NO_3)_2$ solution reflected the original state of Al distribution. Hence, the as-AEI(Na) and as-AEI(Na free) were directly ion-exchanged with 5 mmol/L $Cu(NO_3)_2$ solution, after filtering, washing, drying, and calcination at 550 °C for 10 h, the cal-5Cu/as-AEI(Na) and cal-5Cu/as-AEI(Na free) samples were obtained (Fig. S19). The samples before calcination were marked as 5Cu/as-AEI(Na) and 5Cu/as-AEI(Na free). The chemical composition and acid amount were displayed in Table 2. The Cu content of cal-5Cu/as-AEI(Na) (1.35 wt%) was much higher than that of cal-5Cu/as-AEI(Na free) (0.43 wt%). The Cu ions might mainly exchange with the Na cations in the as-AEI(Na) sample, which has been confirmed by the residual trace amount of Na in the cal-5Cu/as-AEI(Na) sample (Table S3). Simultaneously, by comparing the TG-DTA results of as-AEI(Na) and 5Cu/as-AEI(Na) (Fig. S20a), we found that the lost weight of OSDA slightly decreased from 15.4% to 14.7%, but the peak shape of DTA curves significantly changed. The results illustrated that Cu ions mainly exchanged with the Na cations, simultaneously, OSDA and Na cations rearranged during the Cu-exchange process. When the TG-DTA curves of as-AEI(Na free) and 5Cu/as-AEI(Na free) were compared (Fig. S20b), the close lost weight of OSDA from the TG curves and the similar DTA curves were observed, indicating that the Cu-exchange did not take place with OSDA. We speculated that Cu ions loaded on the as-AEI(Na free) zeolite by physical force or exchanged with the trace OSDA on the surface of the zeolite. The fact that the Cu content of cal-5Cu/as-AEI(Na) was even higher than that of 5Cu/AEI(Na) may be due to the existence of Na, which has been verified in our recent work that more Cu content was

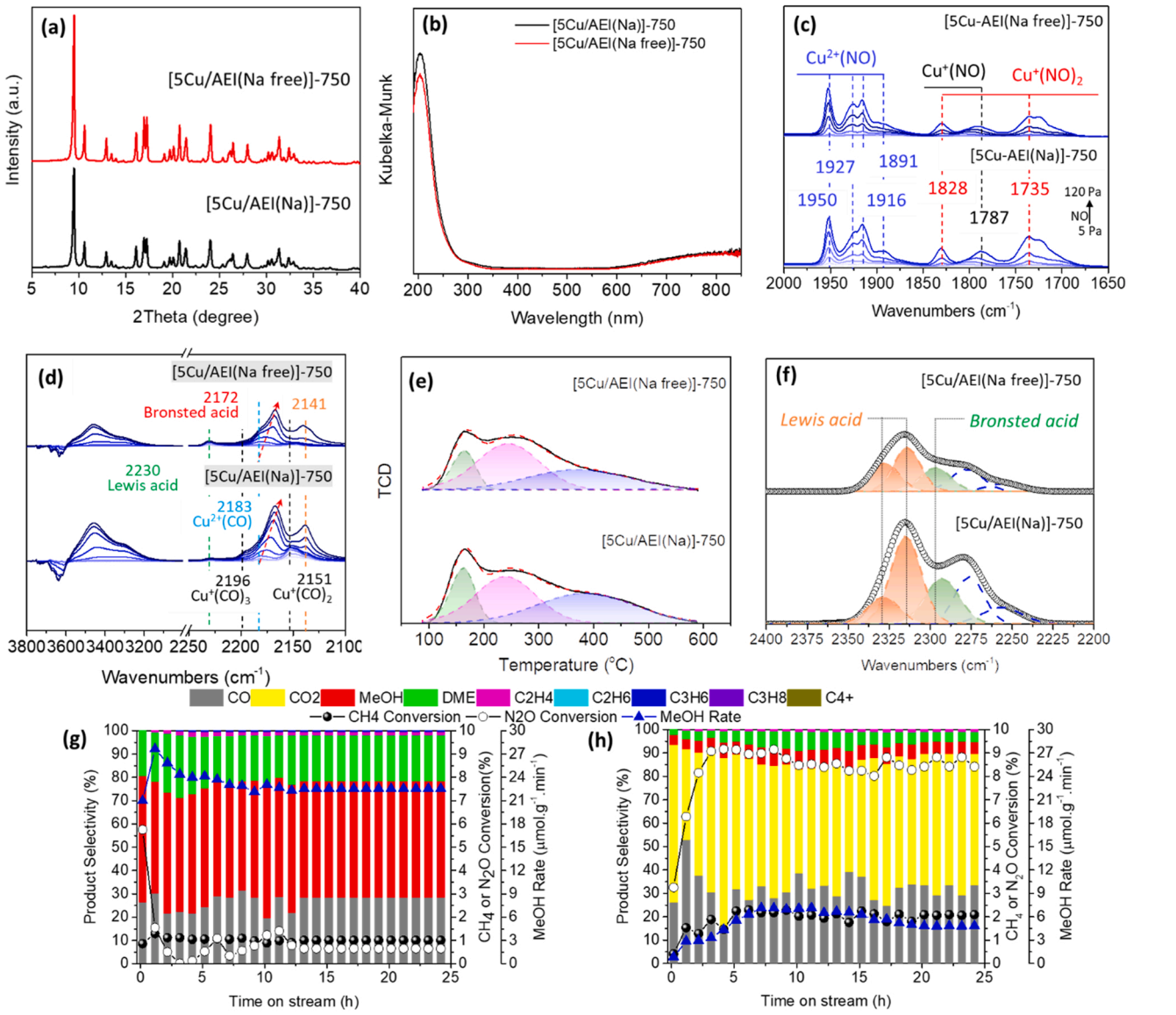

Fig. 8. (a) XRD patterns and (b) UV–vis spectra for [5Cu/AEI(Na)]− 750 and [5Cu/AEI(Na free)]− 750 zeolite catalysts. (c) NO (5–120 Pa) adsorption FTIR spectra and (d) CO (5–1000 Pa) adsorption FTIR spectra over [5Cu/AEI(Na)]− 750 and [5Cu/AEI(Na free)]− 750 zeolite catalysts zeolite catalysts collected at − 120 °C after activation at 500 °C in vacuum for 1 h. (e) NH_3-TPD spectra for [5Cu/AEI(Na)]− 750 and [5Cu/AEI(Na free)]− 750 zeolite catalysts. (f) CD_3CN (200 Pa) adsorption FTIR spectra over [5Cu/AEI(Na)]− 750 and [5Cu/AEI(Na free)]− 750 zeolite catalysts at room temperature after activation at 350 °C in vacuum for 3 h. The performance of (g) [5Cu/AEI(Na)]− 750 and (h) [5Cu/AEI(Na free)]− 750 zeolite catalysts in the cDMTM reaction at 350 °C. Reaction conditions: 100 mg catalyst, $CH_4/N_2O/H_2O/Ar$ = 10/10/2/3 ml·min^{-1}, WHSV = 15000 ml·g^{-1}·h^{-1}.

obtained by ion-exchanging the same concentration of $Cu(NO_3)_2$ solution with Na-type zeolite than the NH_4-type one. The UV–vis spectra (Fig. 7a) demonstrated that both catalysts before and after calcination unveiled the main peaks at 210 nm assignment to the O → Cu^{2+} CT transitions in the isolated Cu species. The UV–vis spectra of both catalysts before calcination demonstrated a distinguished shoulder at 250–275 nm probably attributable to the influence of OSDA on the Cu species. Furthermore, the NO adsorbed FTIR spectra demonstrated the noticeably higher intensity of bands at 1950 and 1925 cm^{-1} for cal-5Cu/as-AEI(Na) zeolite (Fig. 7b). The NH_3-TPD results confirmed the near total amount of acid sites for cal-5Cu/as-AEI(Na) and cal-5Cu/as-AEI(Na free), but different in the amount of weak and strong acid sites (Fig. 7c and Table 2). In comparison with the cal-AEI zeolites (Table S4), the amount of medium and strong acid sites for cal-5Cu/as-AEI(Na) has no significant change, which possibly specified again that the Na cations were ideally replaced by Cu cations. While, in view of cal-5Cu/as-AEI (Na free), the amount of strong acid sites was almost unchanged and the amount of medium acid sites increased in comparison with cal-AEI (Na free) owing to the loaded Cu ions. Fig. 7(d and e) show the performance in cDMTM reaction at 350 °C. The methanol formation rate of cal-5Cu/as-AEI(Na) was up to 27.0 μmol·g^{-1}·min^{-1} with 39% selectivity and stable within 5 h. In the case of cal-5Cu/as-AEI(Na free), the initial methanol formation rate was up to 16.1 μmol·g^{-1}·min^{-1} with 23% selectivity, however, the formed methanol quickly converted to olefins and the methanol formation rate was down to about 1.6 μmol·g^{-1}·min^{-1} with less than 5% selectivity. Fig. 7 f offers the possible loading route of Cu ions on the as-AEI zeolites, in the case of cal-5Cu/as-AEI(Na), Cu ions mainly exchanged with Na cations. The formation of the acid site was the result of the OSDA calcination. As regards the cal-5Cu/as-AEI(Na free), the loaded Cu ions mainly depended on the physical force, during calcination, the location between Cu and OSDA may rearrange.

In addition, the exchange between cal-AEI zeolites and 5 mmol/L Cu $(NO_3)_2$ solution was also implemented (Fig. S21). The Cu content of 5Cu/cal-AEI(Na) (1.35%) was higher than that of 5Cu/cal-AEI(Na free)

(0.85%) due to the existence of Na cation in the cal-AE(Na) zeolite (Table S6). The Cu species of the two samples were simply analyzed by UV–vis spectroscopy (Fig. S22a), which showed the main sharp peak at 210 nm. 5Cu/cal-AEI(Na free) (Fig. S22c) presented the similar reaction performance with 5Cu/AEI(Na free) (Fig. 7 h) because of the analogous Al environment between cal-AEI(Na free) and NH_4-AEI(Na free) zeolites. However, the reaction performance of 5Cu/cal-AEI(Na) (Fig. S22b) was much different from 5Cu/AEI(Na) (Fig. 6b) and cal-5Cu/as-AEI(Na) (Fig. 7d) due to the different environment of Al atoms before Cu-exchange.

3.2.3.3. Improve the catalytic stability. Finally, considering that 5Cu/AEI(Na) and 5Cu/AEI(Na free) achieved the highest methanol formation rate among the *x*Cu/AEI(Na) and *x*Cu/AEI(Na free) zeolite catalysts at 350 °C, respectively, however, each of them was unstable (Figs. 5b and 6 h). Consequently, it is necessary to progress their stability by implementing further calcination at 750 °C for 10 h, the obtained samples were named [5Cu/AEI(Na)]− 750 and [5Cu/AEI(Na free)]− 750 (Fig. S23). The AEI topology structure of the two samples was preserved (Fig. 8a). The UV–vis spectra of both samples were similar (Fig. 8b), showing a sharp band at 210 nm due to the O → Cu^{2+} CT transitions in the isolated Cu species. The NO adsorption FTIR spectra (Fig. 8c) of the two samples exhibited similar features at 1891–1950 cm^{-1}. Noteworthy, the bands at 1887 and 1900 cm^{-1} shifted to 1891 and 1916 cm^{-1} after further calcination at 750 °C for 10 h, which probably demonstrated the agglomeration trend. The CO adsorption FTIR spectra (Fig. 8d) provided the stronger intensity of bands at 2196, 2172, 2151 cm^{-1} for [5Cu/AEI(Na)]− 750, which indicated the higher BAS amount and more Cu species preserved in the cationic states. In the aspect of acidic properties, [5Cu/AEI(Na)]− 750 reserved more amount of strong and weak acid sites than [5Cu/AEI(Na free)]− 750, the amount of medium acid sites for them was akin (Fig. 8e and Table 2). In particular, the amount of BAS and LAS for [5Cu/AEI(Na)]− 750 were higher than that of [5Cu/AEI(Na free)]− 750 (Fig. 8 f and Table S5). The reaction results revealed to us that [5Cu/AEI(Na)]− 750 achieved the maximum 27.7 $\mu mol \cdot g^{-1} \cdot min^{-1}$ methanol formation rate with 48% selectivity and was stable within 25 h (Fig. 8 g), on the other hand, [5Cu/AEI(Na free)]− 750 was also stable, however, the methanol formation rate was only about 5 $\mu mol \cdot g^{-1} \cdot min^{-1}$ with less than 7% selectivity (Fig. 8 h). The catalytic performance in this study was compared with the results reported in the literature (Table S7), a clear advantage in the aspects of MeOH formation rate and selectivity was exhibited by [5Cu/AEI(Na)]− 750 and 5Cu/AEI(Na)− 850 zeolite catalysts.

4. Conclusion

In summary, the AEI-type aluminosilicate zeolites were successfully synthesized in the direction of DMDMP with or without Na cations under the premise of the same total amount of cations. The ^{27}Al MAS NMR, ^{29}Si MAS NMR, and the Co^{2+}-exchange methods emphasized that the location of Al atoms in the framework was highly dependent on the cations. Specifically, the AEI zeolite synthesized with Na cations obtained higher Al content and more Al pairs than the one without Na cations. Thus prepared Cu/AEI zeolites displayed different Cu speciation and acidic properties. When they were applied in the cDMTM reaction at 300–450 °C, the lower activation energy of methane conversion was realized by the Cu/AEI zeolite catalysts synthesized with Na cations. Meanwhile, the Cu/AEI zeolite catalysts synthesized with Na cations accomplished higher methanol formation rate with higher selectivity in the cDMTM reaction at 350 °C. In addition, a series of attempts between the two kinds of zeolites have shown that the environment and the amount of Al in the framework are essential for catalytic activity. The methanol formation rate of 27.3 $\mu mol \cdot g^{-1} \cdot min^{-1}$ with 50% selectivity and stable performance in the cDMTM reaction were provided. Our findings will contribute to the development of the AEI zeolite with the location of Al atoms in the framework controlled to influence the Cu speciation and acidic features, and consequently the reaction performance in the continuous direct oxidation of methane to methanol.

CRediT authorship contribution statement

Peipei Xiao, Yong Wang, Toshiyuki Yokoi conceived and planned the experiments. Peipei Xiao carried out the experiments on the synthesis, characterization of the materials, catalytic application, data processing, data visualization, manuscript writing and revision. Yao Lu measured the NMR. Toshiyuki Yokoi modification the manuscript. All authors provided critical feedback and helped shape the research, analysis and manuscript.

Declaration of Competing Interest

The authors declare that they have no known competing financial interests or personal relationships that could have appeared to influence the work reported in this paper.

Data availability

Data will be made available on request.

Acknowledgments

This work was supported by the INCOE (International Network of Centers of Excellence) project coordinated by BASF SE, Germany. A part of this research was also supported by the JSPS KAKENHI Grant-in-Aid for Scientific Research (B) (No. 21H01714) and JSPS KAKENHI Grantin-Aid for Scientific Research (S) (No. 21H05011). Thanks for Mitsubishi Chemical Corporation to provide us 1,1,3,5-tetramethylpiperidinium hydroxide as the template.

Appendix A. Supporting information

Supplementary data associated with this article can be found in the online version at doi:10.1016/j.apcatb.2023.122395.

References

[1] C.T. Nimlos, A.J. Hoffman, Y.G. Hur, B.J. Lee, J.R.D. Iorio, D.D. Hibbitts, R. Gounder, Experimental and theoretical assessments of aluminum proximity in MFI zeolites and its alteration by organic and inorganic structure-directing agents, Chem. Mater. 32 (2020) 9277–9298.
[2] J. Dedecek, V. Balgova, V. Pashkova, P. Klein, B. Wichterlová, Synthesis of ZSM-5 zeolites with defined distRibution of Al atoms in the framework and multinuclear MAS NMR analysis of the control of Al distribution, Chem. Mater. 24 (2012) 3231–3239.
[3] Y. Shan, W. Shan, X. Shi, J. Du, Y. Yu, H. He, A comparative study of the activity and hydrothermal stability of Al-rich Cu-SSZ-39 and Cu-SSZ-13, Appl. Catal. B: Environ. 264 (2020), 118511.
[4] T. Biligetu, Y. Wang, T. Nishitoba, R. Otomo, S. Park, H. Mochizuki, J.N. Kondo, T. Tatsumi, T. Yokoi, Al distribution and catalytic performance of ZSM-5 zeolites synthesized with various alcohols, J. Catal. 353 (2017) 1–10.
[5] C. Song, Y. Chu, M. Wang, H. Shi, L. Zhao, X. Guo, W. Yang, J. Shen, N. Xue, L. Peng, W. Ding, Cooperativity of adjacent Brønsted acid sites in MFI zeolite channel leads to enhanced polarization and cracking of alkanes, J. Catal. 349 (2017) 163–174.
[6] M. Bernauer, E. Tabor, V. Pashkova, D. Kaucký, Z. Sobalík, B. Wichterlová, J. Dedecek, Proton proximity–New key parameter controlling adsorption, desorption and activity in propene oligomerization over H-ZSM-5 zeolites, J. Catal. 344 (2016) 157–172.
[7] J. Devos, M.L. Bols, D. Plessers, C.V. Goethem, J.W. Seo, S.-J. Hwang, B.F. Sels, M. Dusselier, Synthesis–structure–activity relations in Fe-CHA for C–H activation: control of Al distribution by iNTERZEOLITE CONversion, Chem. Mater. 32 (2019) 273–285.
[8] R. Osuga, S. Bayarsaikhan, S. Yasuda, R. Manabe, H. Shima, S. Tsutsuminai, A. Fukuoka, H. Kobayashi, T. Yokoi, Metal cation-exchanged zeolites with the location, state, and size of metal species controlled, Chem. Commun. (Camb.) 56 (2020) 5913–5916.
[9] C. Paolucci, A.A. Parekh, I. Khurana, J.R. Di Iorio, H. Li, J.D.A. Caballero, A.J. Shih, T. Anggara, W.N. Delgass, J.T. Miller, F.H. Ribeiro, R. Gounder, W.F. Schneider,

Catalysis in a cage: condition-dependent speciation and dynamics of exchanged Cu cations in SSZ-13 zeolites, J. Am. Chem. Soc. 138 (2016) 6028–6048.
[10] P. Sazama, B. Wichterlová, E. Tábor, P. Šťastný, K.S. Naveen, Z. Sobalík, J. Dědeček, S. Sklenák, P. Klein, A. Vondrová, Tailoring of the structure of Fe-cationic species in Fe-ZSM-5 by distribution of Al atoms in the framework for N2O decomposition and NH3-SCR-NOx, J. Catal. 312 (2014) 123–138.
[11] N.M. Phadke, E. Mansoor, M. Bondil, M. Head-Gordon, A.T. Bell, Mechanism and Kinetics of propane dehydrogenation and cracking over Ga/H-MFI prepared via vapor-phase exchange of H-MFI with GaCl3, J. Am. Chem. Soc. 141 (2019) 1614–1627.
[12] N.K. Razdan, A. Kumar, B.L. Foley, A. Bhan, Influence of ethylene and acetylene on the rate and reversibility of methane dehydroaromatization on Mo/H-ZSM-5 catalysts, J. Catal. 381 (2020) 261–270.
[13] I. Pinilla-Herrero, E. Borfecchia, J. Holzinger, U.V. Mentzel, F. Joensen, K. A. Lomachenko, S. Bordiga, C. Lamberti, G. Berlier, U. Olsbye, S. Svelle, J. Skibsted, P. Beato, High Zn/Al ratios enhance dehydrogenation vs hydrogen transfer reactions of Zn-ZSM-5 catalytic systems in methanol conversion to aromatics, J. Catal. 362 (2018) 146–163.
[14] J.M. Findley, P.I. Ravikovitch, D.S. Sholl, The effect of aluminum short-range ordering on carbon dioxide adsorption in zeolites, J. Phys. Chem. C. 122 (2018) 12332–12340.
[15] S. Prodinger, M.A. Derewinski, Y. Wang, N.M. Washton, E.D. Walter, J. Szanyi, F. Gao, Y. Wang, C.H.F. Peden, Sub-micron Cu/SSZ-13: synthesis and application as selective catalytic reduction (SCR) catalysts, Appl. Catal. B: Environ. 201 (2017) 461–469.
[16] M. Dusselier, M.A. Deimund, J.E. Schmidt, M.E. Davis, Methanol-to-olefins catalysis with hydrothermally treated zeolite SSZ-39, ACS Catal. 5 (2015) 6078–6085.
[17] S.J. Kwak, H.S. Kwak, N. Park, Myung-June Park, A.W.B. Lee, Recent progress on Al distribution over zeolite frameworks: linking theories and experiments, Korean J. Chem. Eng. 38 (2021) 1117–1128.
[18] S. Wang, Y. He, W. Jiao, J. Wang, W. Fan, Recent experimental and theoretical studies on Al siting/acid site distribution in zeolite framework, Curr. Opin. Chem. Eng. 23 (2019) 146–154.
[19] T.T. Le, A. Chawla, J.D. Rimer, Impact of acid site speciation and spatial gradients on zeolite catalysis, J. Catal. 391 (2020) 56–68.
[20] B.C. Knott, C.T. Nimlos, D.J. Robichaud, M.R. Nimlos, S. Kim, R. Gounder, Consideration of the aluminum distribution in zeolites in theoretical and experimental catalysis research, ACS Catal. 8 (2018) 770–784.
[21] C. Márquez-Alvarez, A.B. Pinar, R. García, M. Grande-Casas, J. Pérez-Pariente, Influence of Al distribution and defects concentration of ferrierite catalysts synthesized from Na-free gels in the skeletal isomerization of n-butene, Top. Catal. 52 (2009) 1281–1291.
[22] A.B. Pinar, L. Gómez-Hortigüela, L.B. McCusker, J. Pérez-Pariente, Controlling the aluminum distribution in the zeolite ferrierite via the organic structure directing agent, Chem. Mater. 25 (2013) 3654–3661.
[23] J.R.D. Iorio, S. Li, C.B. Jones, C.T. Nimlos, Y. Wang, E. Kunkes, V. Vattipalli, S. Prasad, A. Moini, W.F. Schneider, R. Gounder, Cooperative and competitive occlusion of organic and inorganic structure-directing agents within chabazite zeolites influences their aluminum arrangement, J. Am. Chem. Soc. 142 (2020) 4807–4819.
[24] J.R.D. Iorio, C.T. Nimlosand, R. Gounder, Introducing catalytic diversity into single-site chabazite zeolites of fixed composition via synthetic control of active site proximity, ACS Catal. 7 (2017) 6663–6674.
[25] E.M. Gallego, C. Li, C. Paris, N. Martín, J. Martínez-Triguero, M. Boronat, M. Moliner, A. Corma, Making nanosized CHA zeolites with controlled Al distribution for optimizing methanol-to-olefin performance, Chem. Eur. J. 24 (2018) 14631–14635.
[26] V. Pashkova, S. Sklenak, P. Klein, M. Urbanova, J. Dedecek, Location of framework Al atoms in the channels of ZSM-5: effect of the (hydrothermal) synthesis, Chemistry 22 (2016) 3937–3941.
[27] T. Yokoi, H. Mochizuki, S. Namba, J.N. Kondo, T. Tatsumi, Control of the Al distribution in the framework of ZSM-5 Zeolite and its evaluation by solid-state NMR technique and catalytic properties, J. Phys. Chem. C. 119 (2015) 15303–15315.
[28] Y. Roma, M.M. n-Leshkov, M.E. Davis, Impact of controlling the site distribution of Al atoms on catalytic properties in ferrierite-type zeolites, J. Phys. Chem. C. 115 (2011) 1096–1102.
[29] T. Nishitoba, N. Yoshida, J.N. Kondo, T. Yokoi, Control of Al distribution in the CHA-type aluminosilicate zeolites and its impact on the hydrothermal stability and catalytic properties, Ind. Eng. Chem. Res. 57 (2018) 3914–3922.
[30] V. Pashkova, P. Klein, J. Dedecek, V. Tokarová, B. Wichterlová, Incorporation of Al at ZSM-5 hydrothermal synthesis. Tuning of Al pairs in the framework, Microporous Mesoporous Mater. 202 (2015) 138–146.
[31] V. Gábová, J. Dědeček, J. Čejka, Control of Al distribution in ZSM-5 by conditions of zeolite synthesis, Chem. Commun. 10 (2003) 1196–1197.
[32] M. Dusselier, J.E. Schmidt, R. Moulton, B. Haymore, M. Hellums, M.E. Davis, Influence of organic structure directing agent isomer distribution on the synthesis of SSZ-39, Chem. Mater. 27 (2015) 2695–2702.
[33] N. Zhu, Y. Shan, W. Shan, Z. Lian, J. Du, H. He, Reaction pathways of standard and fast selective catalytic reduction over Cu-SSZ-39, Environ. Sci. Technol. 55 (2021) 16175–16183.
[34] O. Memioglu, B. Ipek, A potential catalyst for continuous methane partial oxidation to methanol using N2O: Cu-SSZ-39, Chem. Commun. 57 (2021) 1364–1367.
[35] B. Ipek, R.F. Lobo, Catalytic conversion of methane to methanol on Cu-SSZ-13 using N2O as oxidant, Chem. Commun. (Camb.) 52 (2016) 13401–13404.
[36] M. Dusselier, M.E. Davis, Small-pore zeolites: synthesis and catalysis, Chem. Rev. 118 (2018) 5265–5329.
[37] N. Tsunoji, D. Shimono, K. Tsuchiya, M. Sadakane, T. Sano, Formation pathway of AEI zeolites as a basis for a streamlined synthesis, Chem. Mater. 32 (2020) 60–74.
[38] R. Ransom, R. Moulton, D.F. Shantz, The structure directing agent isomer used in SSZ-39 synthesis impacts the zeolite activity towards selective catalytic reduction of nitric oxides, J. Catal. 382 (2020) 339–346.
[39] H. Xu, W. Chen, Q. Wu, C. Lei, J. Zhang, S. Han, L. Zhang, Q. Zhu, X. Meng, D. Dai, S. Maurer, A.-N. Parvulescu, U. Müller, W. Zhang, T. Yokoi, X. Bao, B. Marler, D. E. De Vos, U. Kolb, A. Zheng, F.-S. Xiao, Transformation synthesis of aluminosilicate SSZ-39 zeolite from ZSM-5 and beta zeolite, J. Mater. Chem. A 7 (2019) 4420–4425.
[40] K. Narsimhan, K. Iyoki, K. Dinh, Y. Roman-Leshkov, Catalytic Oxidation of methane into methanol over copper-exchanged zeolites with oxygen at low temperature, ACS Cent. Sci. 2 (2016) 424–429.
[41] K.T. Dinh, M.M. Sullivan, K. Narsimhan, P. Serna, R.J. Meyer, M. Dincă, Y. Román-Leshkov, Continuous Partial Oxidation of Methane to Methanol Catalyzed by Diffusion-Paired Cu Dimers in Copper-Exchanged Zeolites, in: J. Am. Chem. Soc, 141, 2019, pp. 11641–11650.
[42] R. Xu, N. Liu, C. Dai, Y. Li, J. Zhang, B. Wu, G. Yu, B. Chen, H2O-built proton transfer bridge enhances continuous methane oxidation to methanolover Cu-BEA zeolite, Angew. Chem. Int. Ed. 60 (2021) 16634–16640.
[43] P. Schwach, X. Pan, X. Bao, Direct conversion of methane to value-added chemicals over heterogeneous catalysts: challenges and prospects, Chem. Rev. 117 (2017) 8497–8520.
[44] W. Zhou, K. Cheng, J. Kang, C. Zhou, V. Subramanian, Q. Zhang, Y. Wang, New horizon in C1 chemistry: breaking the selectivity limitation in transformation of syngas and hydrogenation of CO_2 into hydrocarbon chemicals and fuels, Chem. Soc. Rev. 48 (2019) 3193.
[45] M. Ravi, M. Ranocchiari, J.A. van Bokhoven, The direct catalytic oxidation of methane to methanol—a critical assessment, Angew. Chem. Int. Ed. 56 (2017) 16464–16483.
[46] F. Göltl, S. Bhandari, M. Mavrikakis, Thermodynamics perspective on the stepwise conversion of methane to methanol over Cu-exchanged SSZ-13, ACS Catal. 11 (2021) 7719–7734.
[47] M.A. Newton, A.J. Knorpp, V.L. Sushkevich, D. Palagin, J.A. van Bokhoven, Active sites and mechanisms in the direct conversion of methane to methanol using Cu in zeolitic hosts: a critical examination, Chem. Soc. Rev. 49 (2020) 1449–1486.
[48] J. Dědeček, D. Kaucký, B. Wichterlová, O. Gonsiorová, Co2+ions as probes of Al distribution in the framework of zeolites. ZSM-5 study, Phys. Chem. Chem. Phys. 4 (2002) 5406–5413.
[49] J.K.D. Freude, NMR Tech., Handb. Porous Solids 1 (2002) 465–504.
[50] P. Han, Z. Zhang, Z. Chen, J. Lin, S. Wan, Y. Wang, S. Wang, Critical role of Al pair sites in methane oxidation to methanol on Cu-exchanged mordenite zeolites, Catalysts 11 (2021) 751.
[51] C.-R. Boruntea, L.F. Lundegaard, A. Corma, P.N.R. Vennestrøm, Crystallization of AEI and AFX zeolites through zeolite-to-zeolite transformations, Microporous Mesoporous Mater. 278 (2019) 105–114.
[52] G. Wu, F. Hei, N. Guan, L. Li, Oxidative dehydrogenation of propane with nitrous oxide over Fe–MFI prepared by ion-exchange: effect of acid post-treatments, Catal. Sci. Technol. 3 (2013) 1333–1342.
[53] L.J. Lobree, I.C. Hwang, J.A. Reimer, A.T. Bell, Investigations of the state of Fe in H–ZSM-5, J. Catal. 186 (1999) 242–253.
[54] S. Zhou, F. Tang, H. Wang, S. Wang, L. Liu, Effect of Cu concentration on the selective catalytic reduction of NO with ammonia for aluminosilicate zeolite SSZ-13 catalysts, J. Phys. Chem. C. 125 (2021) 14675–14680.
[55] J. Su, H. Zhou, S. Liu, C. Wang, W. Jiao, Y. Wang, C. Liu, Y. Ye, Y. Zhang, L. Zhang, H. Liu, D. Wang, W. Yang, Z. Xie, M. He, Syngas to light olefins conversion with high olefin/paraffin ratio using ZnCrOx/AlPO-18 bifunctional catalysts, Nat. Commun. 10 (1) (2019) 1–8.
[56] F. Giordanino, P.N. Vennestrom, L.F. Lundegaard, F.N. Stappen, S. Mossin, P. Beato, S. Bordiga, C. Lamberti, Characterization of Cu-exchanged SSZ-13: a comparative FTIR, UV-Vis, and EPR study with Cu-ZSM-5 and Cu-beta with similar Si/Al and Cu/Al ratios, Dalton Trans. 42 (2013) 12741–12761.
[57] Y. Wang, T. Nishitoba, Y. Wang, X. Meng, F.S. Xiao, W. Zhang, H. Gies, B. Marler, D.D. Vos, U. Kolb, M. Feyen, R. McGuire, A.-N. Parvulescu, T. Yokoi, Cu-exchanged CHA-type zeolite from organic template-free synthesis: an effective catalyst for NH3–SCR, Ind. Eng. Chem. Res. 59 (2020) 7375–7382.
[58] A. Kharchenko, V. Zholobenko, A. Vicente, C. Fernandez, H. Vezin, V. De Waele, S. Mintova, Formation of copper nanoparticles in LTL nanosized zeolite: spectroscopic characterization, Phys. Chem. Chem. Phys. 20 (2018) 2880–2889.
[59] P. Sazama, J. Moravkova, S. Sklenak, A. Vondrova, E. Tabor, G. Sadovska, R. Pilar, Effect of the nuclearity and coordination of Cu and Fe sites in beta zeolites on the oxidation of hydrocarbons, ACS Catal. 10 (2020) 3984–4002.
[60] V.L. Sushkevich, D. Palagin, M. Ranocchiari, J.A. van Bokhoven, Selective anaerobic oxidation of methane enables direct synthesis of methanol, Science 356 (2017) 523–527.
[61] D. Palagin, V.L. Sushkevich, A.J. Knorpp, M. Ranocchiari, J.A.van Bokhoven, Mapping vibrational spectra to the structures of copper species in zeolites based on calculated stretching frequencies of adsorbed nitrogen and carbon monoxides, J. Phys. Chem. C. 125 (2021) 12094–12106.
[62] R. Kefirov, A. Penkova, K. Hadjiivanov, S. Dzwigaj, M. Cheb, Stabilization of Cu+ ions in BEA zeolite: Study by FTIR spectroscopy of adsorbed CO and TPR, Microporous Mesoporous Mater. 116 (2008) 180–187.
[63] V. Zdravkova, N. Drenchev, E. Ivanova, M. Mihaylov, K. Hadjiivanov, Surprising coordination chemistry of Cu+ cations in zeolites: FTIR study of adsorption and

coadsorption of CO, NO, N2, and H2O on Cu−ZSM-5, J. Phys. Chem. C. 119 (2015) 15292–15302.

[64] J. Szanyi, F. Gao, J.H. Kwak, M. Kollar, Y. Wang, C.H. Peden, Characterization of Fe(2)(+) ions in Fe,H/SSZ-13 zeolites: FTIR spectroscopy of CO and NO probe molecules, Phys. Chem. Chem. Phys. 18 (2016) us10473–us10485.

[65] Y. Li, M. Wang, S. Liu, F. Wu, Q. Zhang, S. Zhang, K. Cheng, Y. Wang, Distance for communication between metal and acid sites for syngas conversion, ACS Catal. 12 (2022) 8793–8801.